RSC Advances

ROYAL SOCIETY OF CHEMISTRY

www.rsc.org/advances

Journal Name

RSCPublishing

ARTICLE

Mechanical properties of commercial copper current-collector foils

Cite this: DOI: 10.1039/xoxx00000x

Jianyu Zhu[a], Jiemin Feng[b,c], Zhansheng Guo[a,b,*]

Received ooth January 2012,
Accepted ooth January 2012

DOI: 10.1039/xoxx00000x

www.rsc.org/

The functionality and reliability of the current collector (CC) are crucial to design and fabricate electrodes for Li-ion batteries because the CC serves as the bridge between external electronic and internal Li-ion transports. Therefore, understanding the mechanical behavior of CCs is of great importance for battery design and manufacturing. In this paper, we report the measured values of the elastic moduli of six commercial copper current-collector (CCC) foils. Measurements were performed using three techniques: a standard microtensile testing machine equipped with a laser sensor, dynamic mechanical analysis (DMA), and nanoindentation. For electrolytic copper (E-Cu) foils, we find elastic moduli of approximately 70 GPa, and for rolled copper (R-Cu) foils, we find elastic moduli of approximately 50 GPa. Values for yield strength and fracture strength of the foils were determined from load-deflection curves; the results are consistent with values recommended by the manufacturer. Crystalline structures, which influence values for the elastic moduli of the foils, were investigated by X-ray diffraction. Surface morphologies of the foils before testing and the fracture morphologies after testing were studied by scanning electron microscopy.

* Corresponding Author: Z.-S. Guo, Tel: 86-21-56331451, Fax:86-21-36033287, Email: davidzsguo@shu.edu.cn

Journal Name RSCPublishing

ARTICLE

1. Introduction

Lithium-ion batteries (LIBs) play an important role in storing electrical energy. However, most studies on LIB functionality have focused on performance of the cathode, anode, and electrolyte materials[1]. To better understand the degradation mechanisms in LIBs, all components in the battery, including the separator[2] and current collector (CC), must be tested under real-life conditions. In LIBs, copper is used as the CC for the anode and aluminum is used as the CC for the cathode[1]. In recent years, many researchers have studied such degradation mechanisms as diffusion-induced stress and structural volume changes when Li ions are inserted into or extracted from active materials of electrodes[3-10]. In contrast, less attention has been paid to CC foils, which play an important role in the cycle performance of LIBs. Mechanical failure of CC foils in LIBs can result in external electronic transport failures followed by battery failure.

Only a few studies have considered the influence of copper CCs (CCCs) on Li-ion diffusion and diffusion-induced stress. Zhang et al.[3-5] used simulations to study the role of the CC in diffusion-induced stress of active materials of electrodes; however, in their simulation, they just used bulk properties of copper. Gao et al.[11,12] showed that the CC might affect LIB performance. Nagpure et al.[13] studied the influence of copper CCs on LIBs. They found that lithium impurities in the CCC lead to degradation of its thermal and electrical behavior; therefore, such impurities cannot be ignored in efforts to understand aging mechanisms that impact the life and performance of LIBs. Sa et al.[14] found that the CC also plays an extremely important role in rechargeable LIBs. The physical and chemical properties of the CC can impact the performance of LIBs, and use of different CCs can result in significant differences in the performance of LIBs. Kim et al.[15] demonstrated that the cycle life of a silicon–graphite composite electrode was significantly improved by using a CCC with a modified surface morphology. Cho et al.[16] studied the effects of CCC substrates on electrochemical properties of Li/Si thin-film cells. They discovered that the initial capacity depends on microstructures in the copper foil and that cycle performance depends on surface roughness.

Characterizing of the mechanical properties for CCC foils, including elastic moduli, yield strengths, and fracture strengths, should enable more reasonable and reliable LIB designs and manufacturing processes. Although bulk copper is well understood, the same is not true for copper foils. This is because of the intricacies and complexities involved in fabricating the specimens and subsequent handling during testing. Since CCs affect the performance of LIBs, we report experimental results for elastic moduli of CCC foils measured by a microtensile testing machine, dynamic mechanical analysis (DMA), and nanoindentation. These tests were performed on CCC foil samples having six different thicknesses and fabricated via two different processes. Yield strengths and fracture strengths of the CCC foils were obtained from stress–strain curves obtained from the microtensile tests. Crystalline structures and surface morphologies were investigated by X-ray diffraction (XRD) and scanning electron microscopy (SEM), respectively.

2. Experiments

2.1 Materials

All Cu foils used in this investigation had purities of 99.95% and were produced industrially by rolling (R-Cu) (Lingbao Wason Copper Foil Co., Ltd., China and Dongguan Wah Wei Copper Foil Technology Ltd., China) or by electrolytic extraction (E-Cu) (Lingbao Wason Copper Foil Co., Ltd., China and Dongguan Wah Wei Copper Foil Technology Ltd., China). They were tested in their as-received conditions. Sample thickness, manufacturing process, and mechanical properties are summarized in Table 1.

Table 1. Thicknesses and mechanical properties of copper foils tested in this study.

Thickness (μm)	Process	Surface	Tensile strength (MPa)	Elongation (%)
8	E-Cu	Double side shiny	≥295	≥4.0
9	R-Cu	Single side shiny	≥245	≥2.5
12	E-Cu	Double side shiny	≥295	≥5
15	E-Cu	Double side shiny	≥295	≥6
18	R-Cu	Single side shiny	≥245	≥5
35	R-Cu	Single side shiny	≥245	≥5

2.2 Microtensile tests

Tensile properties were determined using a microtensile testing machine (Zwick/roll Germany, load capacity between 10 and 2000 N) equipped with a laser sensor. To avoid the influence of detrimental vibrations, the entire testing machine was mounted on an optical table. CCC foils were glued to specially designed grips and were aligned using an x-y die. A double-bladed cutter was used to prepare specimens according to the ASTM standard E345-93 (2008)[17]. If necessary, cutting edges of the double-bladed cutter (D-tx003, Ningbo Donrie Metal Manufacture Co., Ltd, China) should be lubricated with a material such as stearic acid in alcohol or a similar alternative. The finished specimens were examined under approximately 20× magnification to determine whether edges were smooth and that there were no surface scratches or creases. Specimens

showing discernible surface scratches, creases, or edge discontinuities were rejected. Detailed descriptions of the noncontact optical method can be found in numerous other researches[18-20].

2.3 Dynamic mechanical analysis tests

Elastic moduli can also be determined using a dynamic mechanical analysis machine (TA Instruments DMA Q800). Uniaxial testing clamps were used. A double-bladed cutter (D-tx003, Ningbo Donrie Metal Manufacture Co., Ltd, China) was used to cut specimens from the foils to the desired dimensions: 60 mm × 3 mm × varying thickness. A very small preload was applied to the samples to ensure that the specimens were always in tension. All samples were tested at a frequency of 1 Hz.

2.4 Nanoindentation tests

Nanoindentation techniques have been developed for probing mechanical properties of materials and have become popular experimental techniques. Our nanoindentation tests were conducted using a Hysitron TriboIndenter (Hysitron Inc., Minneapolis, MN, USA) with the continuous stiffness measurement option under constant strain-rate control. The tip on the nanoindenter system was a Berkovich diamond tip, which is preferred for low-load indentation testing. Measurements were performed by loading to the maximum load, then unloading to 95% and holding for 50 s to allow for the thermal-drift correction of the sample, and then unloading completely. The elastic modulus of each specimen was determined from the load–displacement curve using Fischer-Cripps method[21].

2.5 Crystalline structure and surface morphology characterizations

Crystalline structures and crystallographic orientations of the CCC foils were determined using grazing incident-angle XRD (18kW D/MAX2550, Rigaku, Japan). The power of the XRD (Cu Ka radiation) was fixed at 40 kV and 25 mA. The angle of the incident X-ray beam was fixed at 0.5°. To compare diffraction intensities of different sputtering samples, the XRD diffraction angle (2θ) was spanned from 30° to 100°. Surface morphologies of the CCC foils were determined by a desktop scanning electron microscope (Sh3000, Hirox, Korea) before and after tensile testing.

3. Results and discussion

3.1 Elastic modulus

Figures 1–3 show typical stress–strain curves (load–displacement curves) for E-Cu and R-Cu CC foils obtained by microtensile, DMA, and nanoindentation tests, respectively. Copper foils of all six thicknesses had similar stress–strain curves (not shown here). For each specimen, six samples were subjected to tensile testing, three were subjected to DMA, and three indents were used for nanoindentation. Elastic moduli of the CCC foils were determined in the linear elastic region of the stress–strain curves from the microtensile test machine. The resulting values for elastic moduli are shown in Table 2. Figure 1 shows that stress–strain curves were all reproducible, especially when the strain was below 1%. Figures 2(a) and 2(b) show that elongation of the E-Cu foils was larger than those of R-Cu foils. Table 2 shows that the elastic moduli of all CCC foils were much different from that of bulk copper (for bulk Cu, a value in the range 110–126 GPa is usually as assumed in [19, 22]). According to Mechant et al.[22,23], differences in texture explain variations in experimentally determined elastic moduli from 68 GPa up to 132 GPa. The texture of the copper foils in our study was studied by XRD and will be discussed below. Our results indicate that the elastic moduli for CCC foils cannot be replaced with the value for bulk Cu in calculations that predict diffusion-induced stress or fracture of electrodes in LIBs. Table 2 shows that the elastic moduli from different test methods agree reasonably well; i.e., elastic moduli obtained from stress–strain curves of microtensile tests have excellent reliability. A comparison of the elastic moduli of E-Cu (8 μm, 12 μm, and 15 μm) with those of R-Cu (9 μm, 18 μm, and 35 μm) shows that E-Cu foils have higher elastic moduli (approximately 70 GPa) than R-Cu foils (approximately 51 GPa).

Table 2. Test results for elastic moduli of CCC foils.

Thickness (μm)	Elastic modulus (GPa)		
	Microtensile test	DMA test	Nanoindentation test
	Six sample values average	Three sample values average	Three indents values average
8	68	71	70
9	53	51	52
12	69	70	68
15	71	67	72
18	50	49	48
35	56	52	54

3.2 Yield Strength and Fracture Strength

Figure 4 shows the yield strengths for CCC foils having six different thicknesses, and Figure 5 does the same for the fracture strength. Figure 4 shows that decreases in foil thickness significantly increased yield strength, while Figure 5 shows that decreases in thickness had little influence on fracture strength. Since the grain size of thin foil is smaller than the corresponding foil thickness, the foil in the thickness direction may contain few grains. Thus, the increase in the yield strength can be attributed to a grain size effect, as described by the Hall–Petch relationship. The measured fracture strengths were consistent with the values provided by the manufacturer.

Figure 6 shows the elongations of E-Cu and R-Cu CCC foils with different thicknesses. For the same fabrication process, elongation decreased remarkably with decreasing foil thickness, indicating that the plasticities of thicker foils were better than

those of the thinner ones. The larger plasticities of thicker foils can be attributed to the larger grains in those foils, and to more movable dislocations stored in the grains compared to those in the thinner foils. However, the thinner foils contained relatively fewer dislocation sources, which resulted in higher breaking stresses. The measured elongations of all samples were in good agreement with those provided by the manufacturer.

3.3 Crystalline structure characterization

Figure 7 shows the XRD patterns obtained from CCC foils. Five peaks have been observed and compared with the standard powder diffraction card of JCPDS, copper file No. 04-0836. The XRD study confirms that these foils are FCC coppers. Figure 7(a) shows the XRD results of the three different thicknesses of E-Cu CC foils. All E-Cu CC foils were found to be highly textured in the (111) and (200) planes while the intensity peak value of (220) plane was weak. Figure 7(b) shows that all R-Cu CC foils were also highly textured in the (111) and (200) planes with a strong (220) plane. Note that the 35-μm-thick R-Cu CC foil shows a texture-like structure formed along a certain direction because it only has a strong peak in the (220) plane. According to the results of Sarada et al.[24], the foils with a strong peak in the (111) plane had high electrical conductivity, which is the key factor for use as CC in LIBs. This may be a reason why most commercial industries often select E-Cu foils and not R-Cu foils for anode CCs. Of course, R-Cu foils are usually used in devices in which the electrical conductivity requirement is a little lower than that of a battery.

Many microstructure factors, such as crystallographic texture, grain size, grain orientation, grain boundaries, and structural defects, have important influence on mechanical properties, such as hardness, Young's modulus, yielding strength, and fracture toughness[25-31]. Here, we just provide a simple qualitative analysis of crystallographic texture on Young's modulus on the basis of the XRD results. The theoretical calculation and quantitative analysis of microstructure factors affecting mechanical properties which need more are being studied by additional experiment methods. Crystallographic textures have a significant effect because the elastic modulus of copper is direction specific[26]. For example, the Young's modulus (the stiffness of a material in tension) of a copper single crystal varies from 67 GPa (low value) (<100> direction) to 192 GPa (high value) (<111> direction) depending on orientation. In contrast polycrystalline copper has the same modulus of 111 GPa in all directions[32]. The elastic modulus of a (1**) plane is higher than that of a (2**) plane. i.e., the (111) plane, which has the lowest surface energy when an fcc structure dominates the crystal[25], has the highest elastic modulus. From the XRD patterns of our CCC foils (figure 7), the intensity of (111) or (200) plane of E-Cu CC foils is found to be much higher than that of R-Cu foils. For example, the minimum peak value of E-Copper is 106647 cps (8μm) while the maximum peak value in (111) of R-Copper is 53920 cps (18μm); this is likely an important reason why the elastic moduli of E-Copper are higher than those of R-Cu foils. Notably, the elastic modulus measured by the microtensile and DMA tests is a mixed modulus over all crystal planes. In contrast, elastic moduli determined by the nanoindentation test are more discrete than macroscopic test methods because the indenter size is at nanoscale.

3.4 Surface morphology characterization

The Surface morphologies of the CCC foils are shown in Figure 8. The figure shows that surface morphologies were very different depending on whether the surface was shiny or matte. These differences mean that the bonding mechanisms of CCC surfaces with active materials will differ depending on the method of surface treatment. The influence of different surface treatments on electrochemical performance and interfacial bonding strength of electrodes needs further study.

Figures 9(a) and 9(b) present SEM images of surface morphologies close to the fracture zones of the 15-μm-thick E-Cu and 9-μm-thick R-Cu CC foils, respectively. Figure 9(a) is for an E-Cu CC foil and reveals typical knife-edge fracture morphology, while Figure 9(b) is for an R-Cu CC foil and is characterized by a strong crystallographic appearance. Extensive slip bands appear in the 9-μm-thick foil (Figure 9(b)), but only faint slip traces appear in the 15-μm-thick foil (Figure 9(a)). This type of failure was observed for all samples, irrespective of their thicknesses. More detailed analyses of fracture mechanisms are under study.

Conclusions

Elastic moduli of commercial CCC foils were determined using microtensile, DMA, and nanoindentation techniques. Yield strengths, fracture strengths, and elongations were determined using a standard microtensile testing machine equipped with a laser sensor. For the E-Cu foils, the measured elastic moduli were approximately 70 GPa, while those for the R-Cu foils were approximately 50 GPa. Crystalline structures and surface morphologies of the CCC foils were investigated by XRD and SEM, respectively. These results for mechanical properties (elastic modulus, yield strength, fracture strength, and elongation), microstructures, and surface morphologies should contribute to building models for studying battery performance. Only by using such measured values can accurate estimates be established for the performance of LIBs. Even though specific mechanisms for some of the studied phenomenon remain elusive, the measured values and behaviors should contribute to predictions of the cycle life of LIBs.

Acknowledgements

The authors gratefully acknowledge the financial supports by the Science and Technology Commission of Shanghai Municipality (No. 12ZR1410200), the National Science Foundation of China (No. 11472165, 11332005), Shanghai Municipal Education Commission (No. 13ZZ070) and Shanghai leading Academic Discipline Project (No. S30106).

Notes and references

[a] Shanghai Institute of Applied Mathematics and Mechanics, Shanghai University, Shanghai 200072, China.
[b] Shanghai Key Laboratory of Mechanics in Energy Engineering, Shanghai University, Shanghai 200072, China
[c] Department of Mechanics, College of Science, Shanghai University, Shanghai 200072, China

1. C. Daniel and J. O. Besenhard. Handbook of Battery Materials (2nd Edition), 2011 Wiley-VCH Verlag & Co. KGaA, Boschstr. 12, 69469 Weinheim, Germany
2. J. Chen, Y. Yan, T. Sun, Y. Qi, X. Li (2014) Deformation and fracture behaviors of microporous polymer separators for lithium ion batteries. RSC Adv., 4:14904.
3. J Zhang, B Lu, Y Song, X Ji (2012) Diffusion induced stress in layered Li-ion battery electrode plates. Journal of Power Sources, 209:220-227.
4. B Lu, YC Song, ZS Guo, JQ Zhang (2013) Analysis of delamination in thin film electrodes under galvanostatic and potentiostatic operations with Li-ion diffusion from edge. Acta Mechanica Sinica, 29 (3):348-356.
5. Y Song, X Shao, Z Guo, J Zhang (2013) Role of material properties and mechanical constraint on stress-assisted diffusion in plate electrodes of lithium ion batteries. Journal of Physics D: Applied Physics, 46 (10):105307.
6. I. Ryu, J. W. Choi, Y. Cui, W. D. Nix (2011) Size-dependent fracture of Si nanowire battery anodes, Journal of the Mechanics and Physics of Solids, 59:1717.
7. K. Zhao, M. Pharr, J. J. Vlassak and Z. Suo (2010) Fracture of electrodes in lithium-ion batteries caused by fast charging. Journal of Applied Physics. 108:073517.
8. M. Pharr, Z. Suo, J. J. Vlassak (2013) Measurements of the Fracture Energy of Lithiated Silicon Electrodes of Li-ion Batteries. Nano Letters, 13(11):5570-5577.
9. G. Bucci, S. P. V. Nadimpalli, V. A. Sethuraman, A. F. Bower, P. R. Guduru (2014) Measurement and modeling of the mechanical and electrochemical response of amorphous Si thin film electrodes during cyclic lithiation. Journal of the Mechanics and Physics of Solids, 62:276-294.
10. H. Haftbaradaran, X. Xiao, M. W. Verbrugge and H. Gao (2012) Method to deduce the critical size for interfacial delamination of patterned electrode structures and application to lithiation of thin-film silicon islands, Journal of Power Sources, 206:357–366.
11. H. Haftbaradaran, X. Xiao and H. Gao (2013) Critical film thickness for fracture in thin-film electrodes on substrates in the presence of interfacial sliding, Modelling and Simulation in Materials Science and Engineering, 21:074008.
12. M. E. Stournara, X. Xiao, Y. Qi, P. Johari, P. Lu, B. W. Sheldon, H. Gao and V. B. Shenoy (2013) Li segregation induces structure and strength changes at the amorphous Si/Cu interface, Nano Letters, 13(10): 4759–4768.
13. S.C. Nagpure, R. G. Downing,B.Bhushan, and S.S. Babu (2012) Discovery of lithium in copper current collectors used in batteries. Scripta Materialia 67:669–672.
14. Q.N. Sa, and Y. Wang (2012) Ni foam as the current collector for high capacity C–Si composite electrode J. Power Sources, 208:46-51.
15. Y.L. Kim, Y.K. Sun, S.M. Lee (2008) Enhanced electrochemical performance of silicon-based anode material by using current collector with modified surface morphology. Electrochim. Acta, 53:4500-4504.
16. G. B. Cho, B. K. Lee, W. C. Sin, K. K. Cho, H. J. Ahn, T. H. Tae, K. W. Kim (2006) Effects of Cu current collector as a substrate on electrochemical properties of Li/Si thin film cells. Journal of Materials Science, 41:313-315.
17. Standard Test Methods of Tension Testing of Metallic Foil. E345 – 93 (Reapproved 2008).
18. B. Weiss, V. Gröger, G. Khatibi, A. Kotas, P. Zimprich, R. Stickler, B. Zagar (2002) Characterization of mechanical and thermal properties of thin Cu foils and wires. Sensor and Actuators A, 99:172-182.
19. H. D. Merchant, G. Khatibi, B. Weiss (2004) Elastic and elastoplastic response of thin copper foil. Journal of Materials Science, 39:4157-4170.
20. H. D. Merchant, B. Weiss, G. Khatibi (2001) Fatigue and fracture properties of thin metallic foils. International Journal of Fracture, 109:69-89.
21. A. C. Fischer-Cripps (2007) Illustrative Analysis of Load-Displacement Curves in Nanoindentation. J. Mater. Res., 22(11):3075-3086.
22. D. Ma, K. Xu, J. He, J. Lu (1999) Evalution of the mechanical properties of thin metal films. Surface and Coatings Technology, 116-119:128-132.
23. D. J. Dunstan, J. U. Galle, X. D. Hou, K. M. Y. P'ng, A. J. Bushby, B. Yang, D. Kiener (2012) Yield and plastic flow of soft metals in small volumes loaded in tension and flexure. Philosophical Magazine, 92:3199-3215.
24. B. V. Sarada, Ch. L. P. Pavithra, M. Ramakrishma, T. N. Rao, G. Sundararajan (2010) Highly (111) textured copper foils with high hardness and high electrical conductivity by pulse reverse electrodeposition. Electrochemical and Solid Letters, 13:D40-D42.
25. D. A. Porter and K. E. Easterling, in "Phase Transformation in Metals and Alloys", Chapman & Hall, London, 1992
26. J. H. Choi, S. Y. Kang, and D. N. Lee (2000) Relationship between deposition and recrystallization textures of copper and chromium electrodeposits. Journal of Materials Science, 35(16):4055-4066.
27. W. C. Overton Jr. and J. Gafney (1955) Temperature Variation of the Elastic Constants of Cubic Elements. I. Copper. Physical review, 98:969-977.
28. B. Merle, E. W. Schweitzer, and M. Göken (2012), Thickness and grain size dependence of the strength of copper thin films as investigated with bulge tests and nanoindentations. Philosophical Magazine, 92(25–27):3172–3187.
29. J. D. Giallonardo, U. Erb, K.T. Aust, and G. Palumbo (2011) The influence of grain size and texture on the Young's modulus of nanocrystalline nickel and nickel–iron alloys, Philosophical Magazine, 91(36):4594–4605.
30. S. J. Skrzypek, W. ratuszek, A. Bunsch, et al (2010), Crystallographic texture and anisotropy of electrolytic deposited copper coating analysis. journal of Achievements in Materials and manufacturing Engineering, 43:264–268.
31. D. E. J. Armstrong, A. J. Wilkinson, and S. G. Roberts (2009), Measuring anisotropy in Young's modulus of copper using

microcantilever tesing. Journal of Materials Research, 24:3268–3276.

32. http://www.aem.umn.edu/people/faculty/shield/c1b1/pcb4.htm

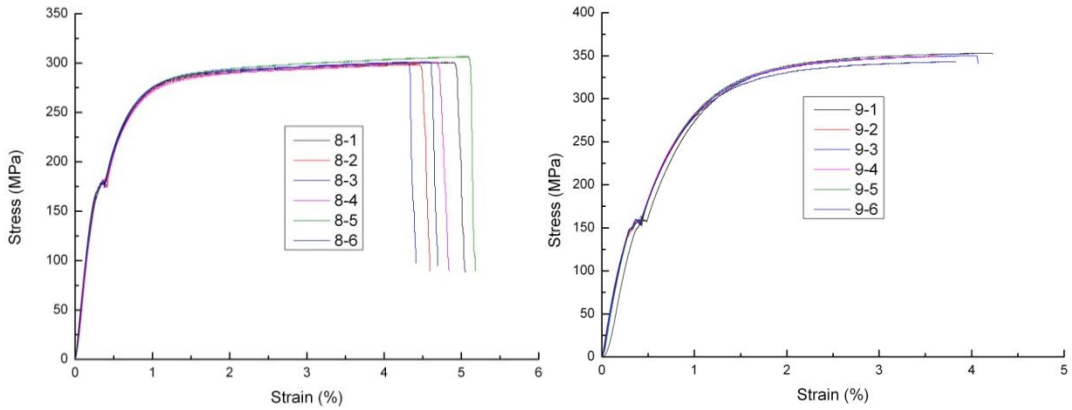

(a) 8 μm E-Cu foils (b) 9 μm R-Cu foils

Figure 1 Typical stress-strain curves of CCC foils by microtensile test

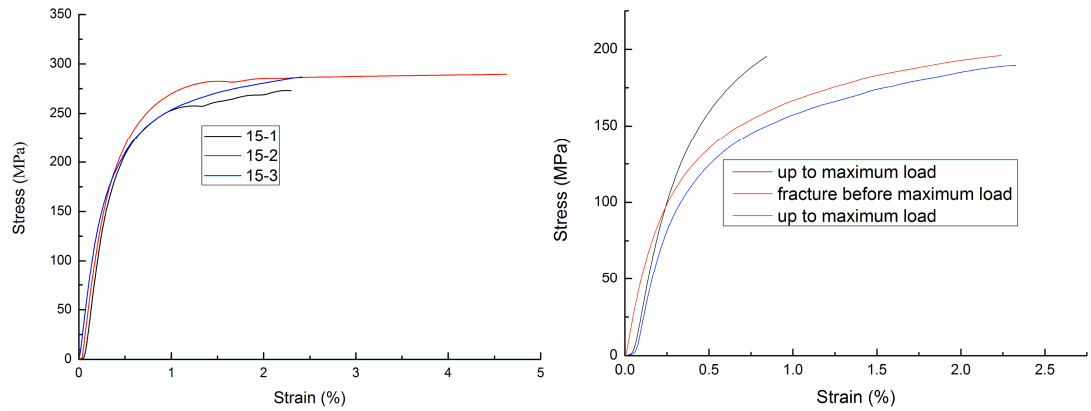

(a) 15 μm E-Cu foils (b) 35 μm R-Cu foils

Figure 2 Typical stress-strain curves of CCC foils by DMA test

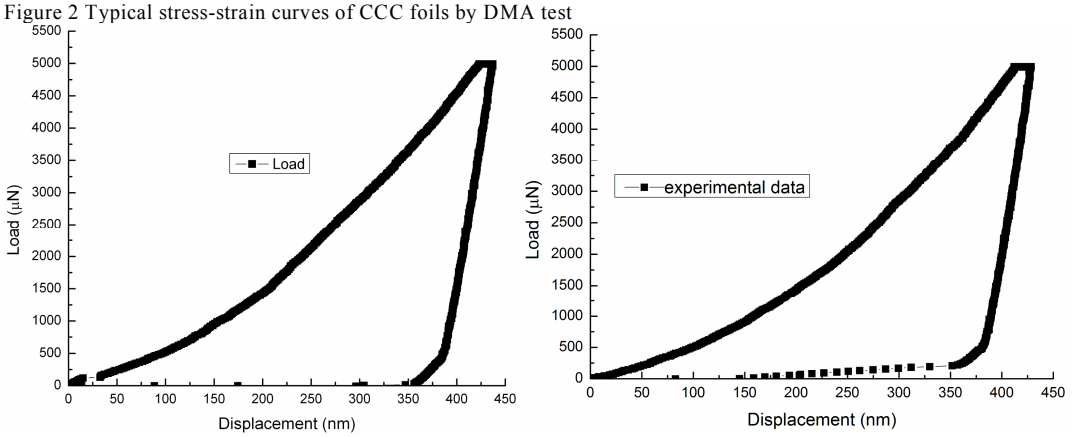

(a) 12 μm E-Cu foils (b) 35 μm R-Cu foils

Figure 3 Load-displacement curves of CCC foils by nanoindentation test

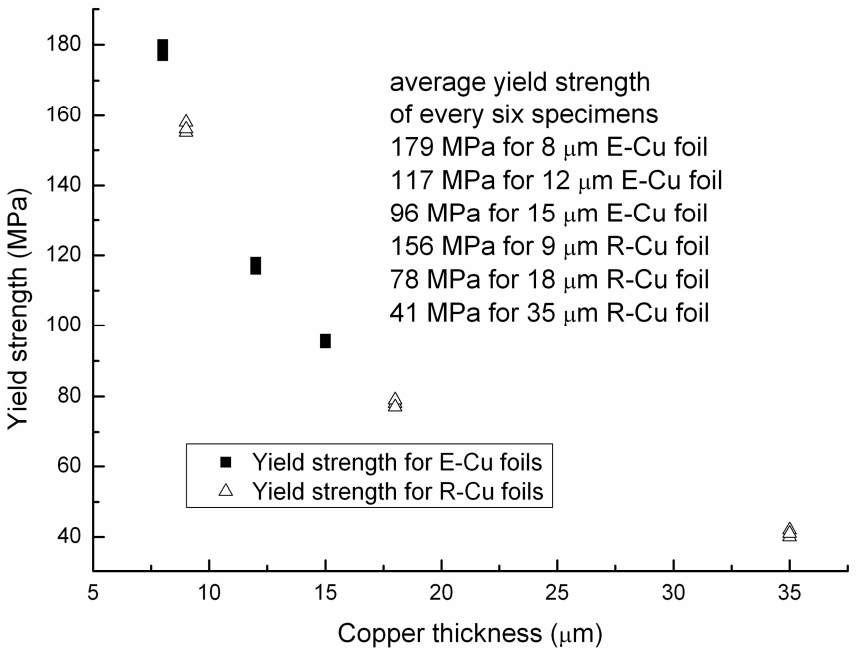

Figure 4 Yield strength of CCC foils as a function of thickness

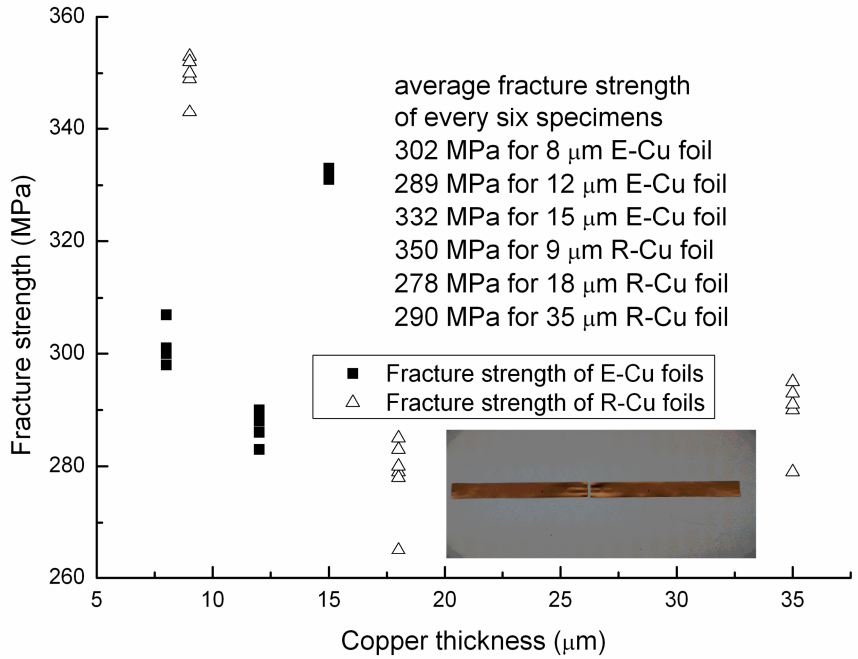

Figure 5 Fracture strength of CCC foils as a function of thickness. The inset is the real picture of sample after microtensile test.

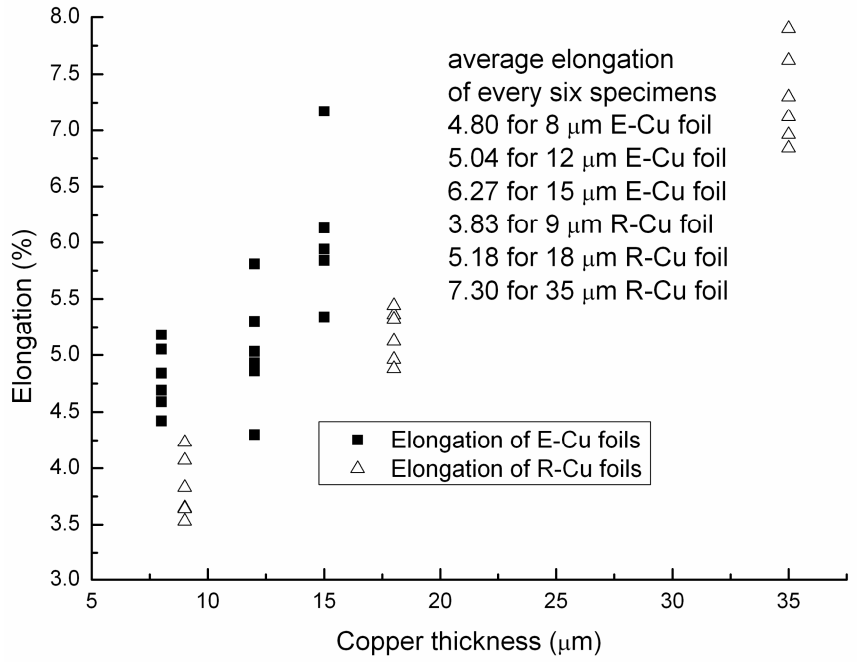

Figure 6 Elongation of CCC foils as a function of thickness

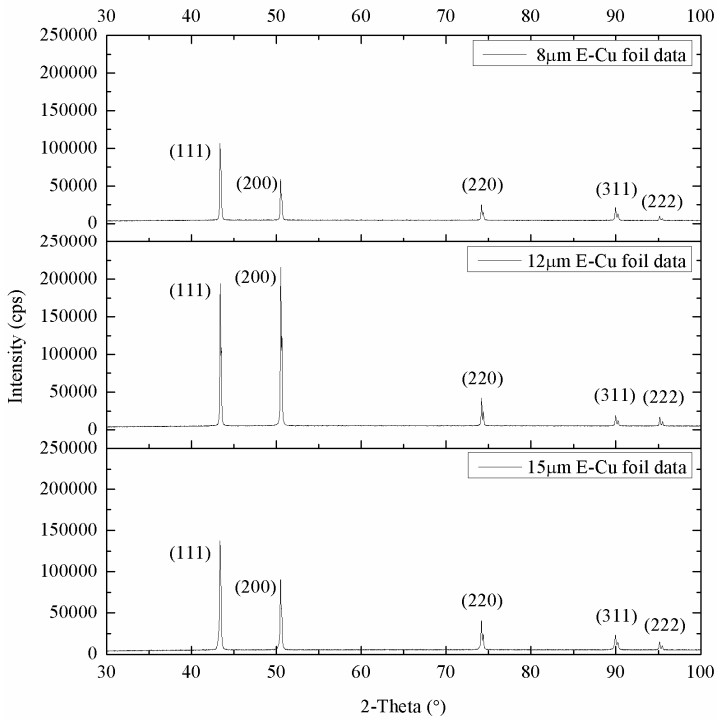

(a) E-Cu foils XRD data

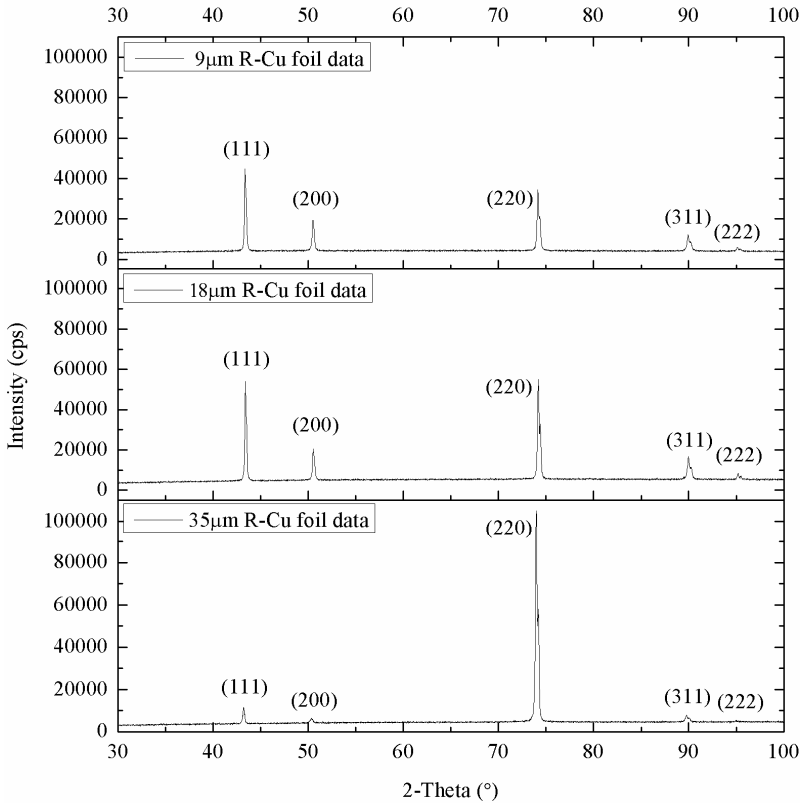

(b) XRD spectra for R-Cu foils XRD data

Figure 7 XRD patterns of CCC foils

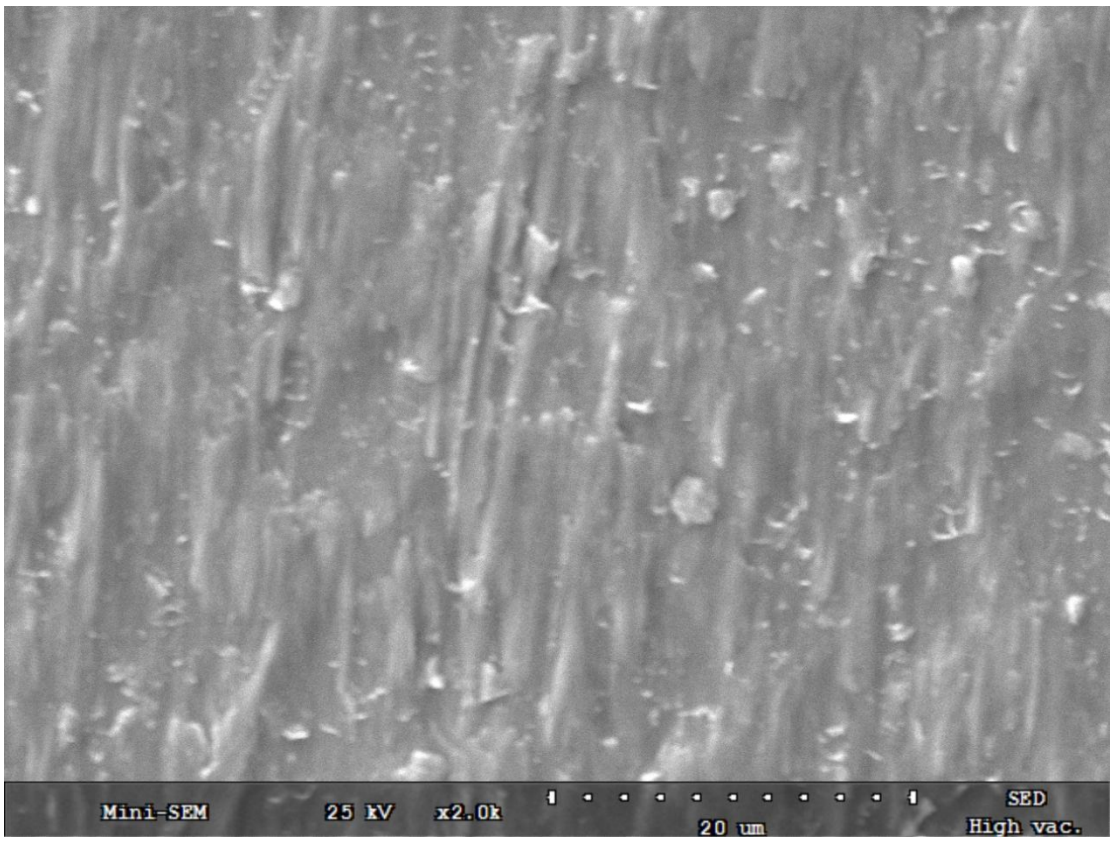

(a) SEM photo of shining-treated side of CCC foils

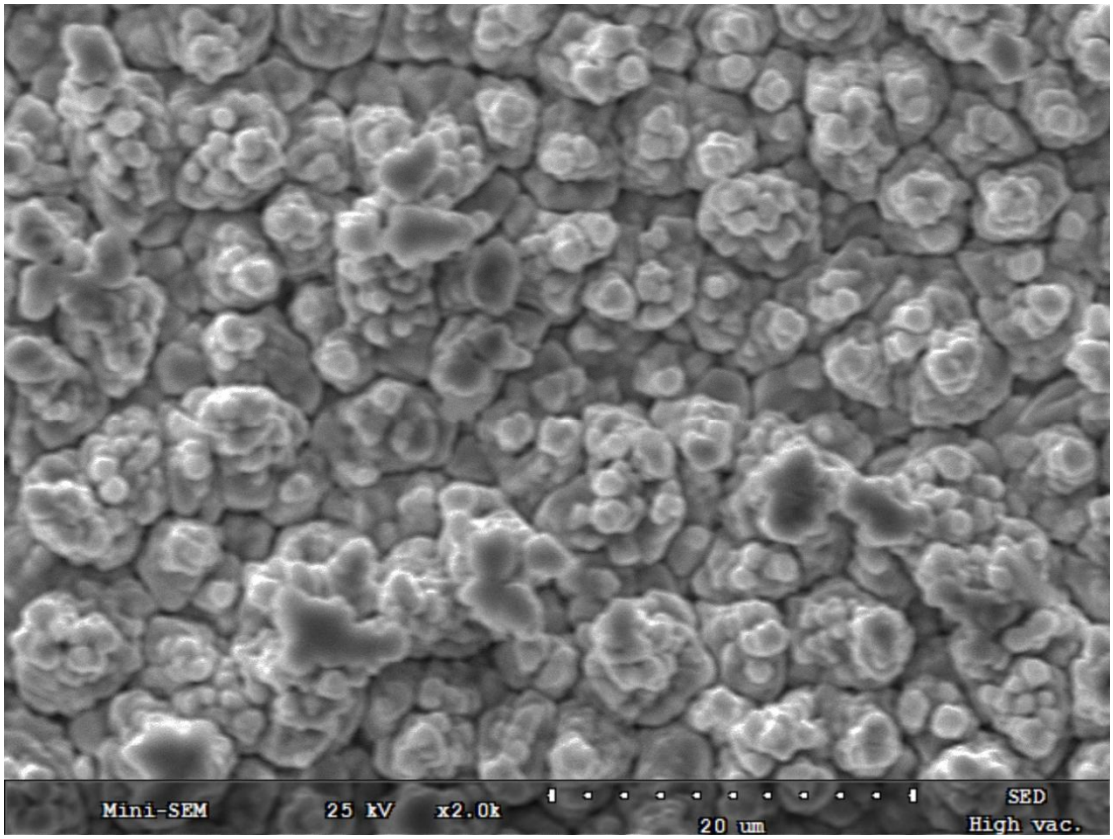

(b) SEM photo of matte-treated side of CCC foils

Figure 8 Typical SEM photographs of CCC foils

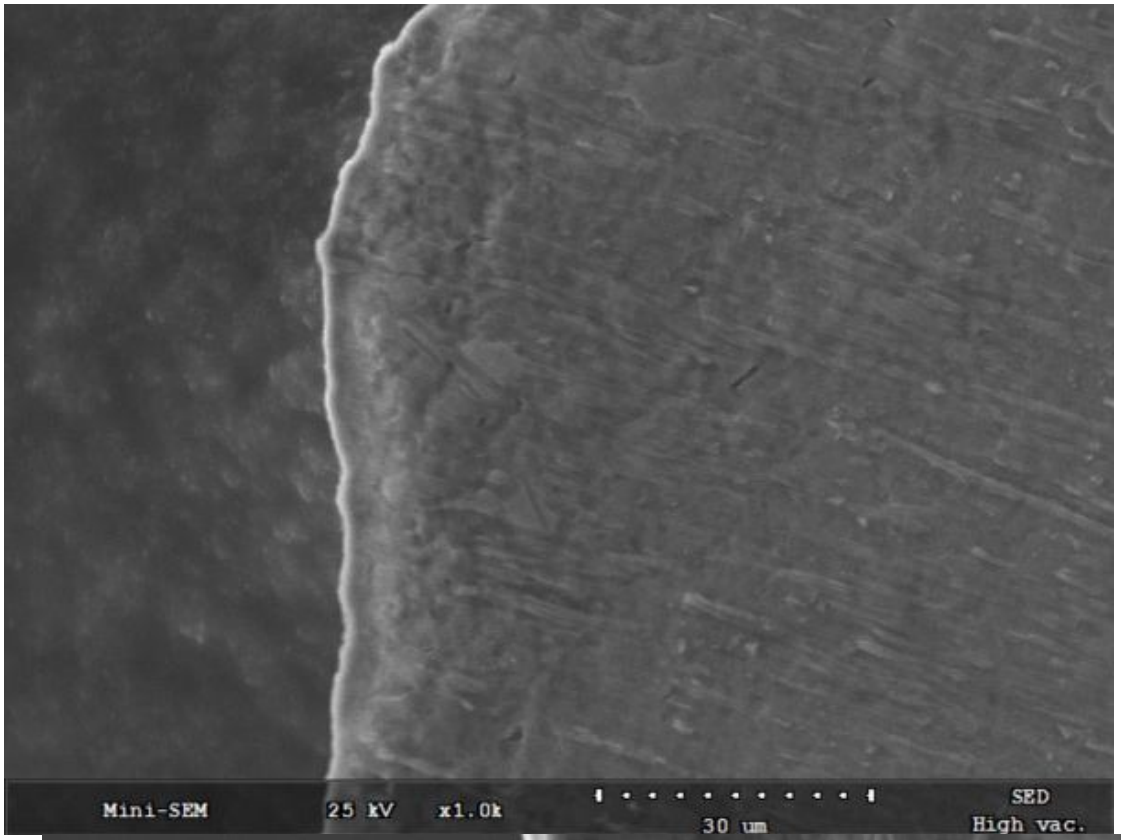

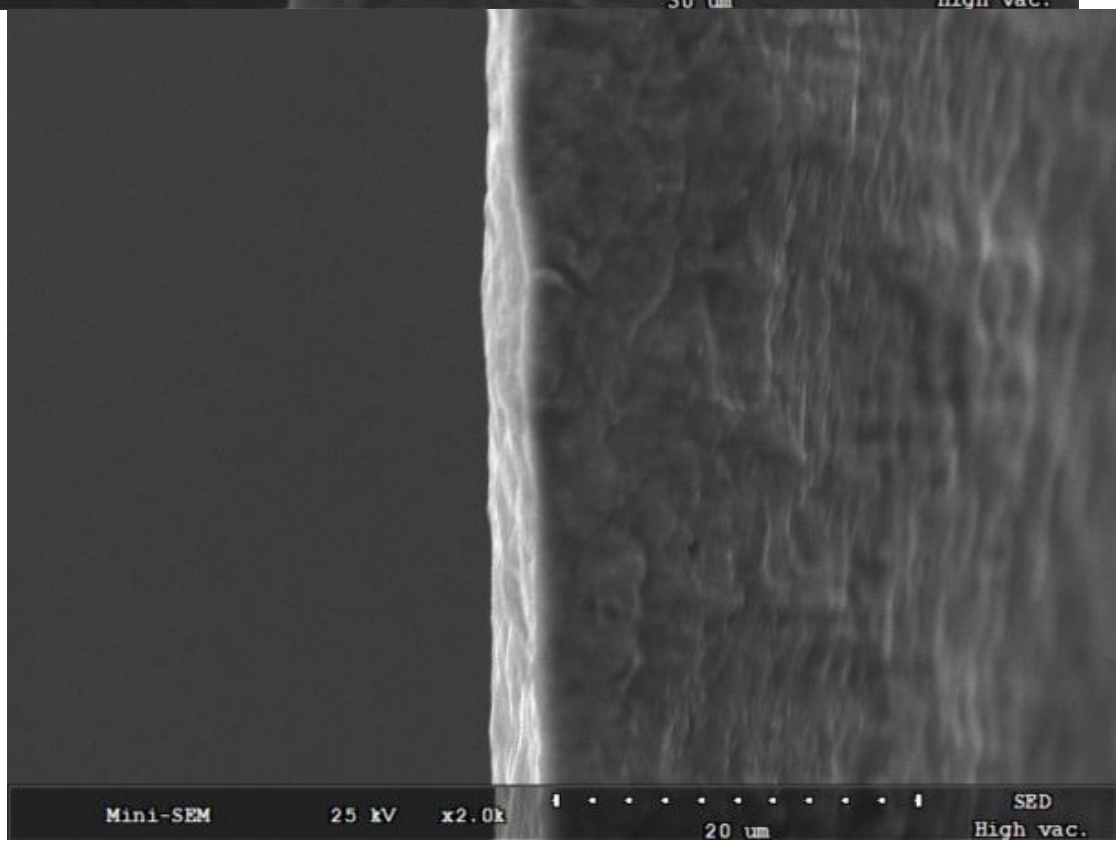

(a) 15 µm E-Cu current collector foil

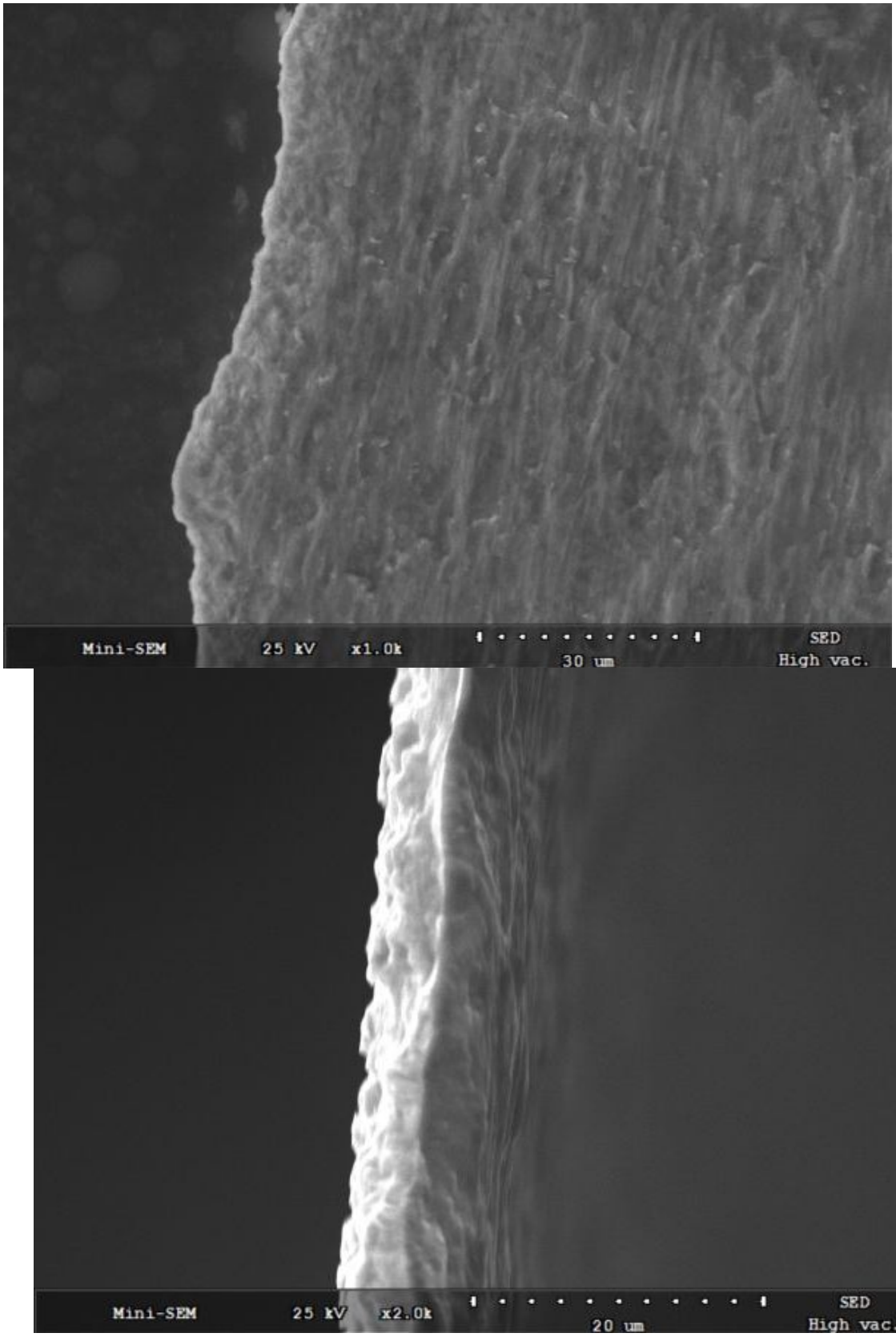

(b) 9 µm R-Cu current collector foil

Figure 9 SEM fractographs of CCC foils tensile tested